A Numerical Simulation of Quench Propagation in Nb₃Sn Cables Covered With Protection Heaters

S. Bakrani Balani ⓘ, T. Salmi ⓘ, V. Calvelli ⓘ, H. Felice ⓘ, and E. Rochepault ⓘ

Abstract—**Superconducting magnets are crucial components in various scientific, industrial, and medical applications, offering unparalleled high magnetic fields and energy efficiency. However, the transition from the superconducting to the normal state, known as a quench, can pose significant challenges due to the sudden local release of stored energy and damage to the magnet system. Quench protection strategies have emerged as essential mechanisms to mitigate the adverse effects of quenches. One of the commonly used methods in accelerator magnets is to use strip heaters on coil surfaces. The heater element length and configuration influence the performance of the quench protection. The study of the quench protection by heaters requires the coupled modelling of the Joule heating, normal zone propagation, and transferring heat from the heaters to the cable. In this article, we present a new 2D finite element simulation model to model the increase of the cable resistance under different heater lengths in Nb₃Sn accelerator magnets. The model allows analyzing heaters with several different lengths of heating stations along the cable. This strategy can be used to maximize the cable resistance increase at high operation current while still providing the needed normal zone propagation at lower currents. We demonstrate the model use with a high-field racetrack dipole model.**

Index Terms—**Accelerator magnets, Nb₃Sn dipoles, numerical simulation, protection heaters, quench protection.**

I. INTRODUCTION

HIGH magnetic field Nb₃Sn dipoles are currently under development for the next generation of particle accelerator magnets. The new dipole magnet generation provides a higher magnetic field allowing to bend higher energy particle beam and increasing their collision energy in the experiments [1]. The phenomenon of quench, characterized by the sudden loss of superconductivity in a magnet's conductor, is a critical safety consideration in the design and operation of the magnets. Early quench detection and a prompt protection system response is essential to limit the local temperature increase and to avoid conductor damage [2]. After quench detection, the magnet energy must be discharged quickly. In accelerator magnets, when

external energy extraction is not sufficient, or not possible, magnets must absorb the stored energy within the windings.

To induce uniform distribution of the energy, it is necessary to rapidly spread the normal zone across the windings. A strip heater-based protection refers to resistive metal heaters that are attached close to the superconducting coils. The purpose of the heater strips is to heat a large fraction of the coil above the critical temperature (T_c) and allow a uniform dissipation of the magnet stored energy in the windings [3]. The heater arrangement highly influences the performance of the quench protection [4], [5]. Often a heater strip includes a-few-centimeters-long heating stations, which are distributed periodically along the length of the coils.

At Tampere University, a 2D numerical simulation has been developed using COMSOL Multiphysics 6.1 in order to study the normal zone propagation velocity (NZPV) in the cable between discrete heating stations. The studied modeling domain includes the cable, heater, and the associated insulation layers with their thicknesses varying from μm scale to mm scale. The variation in the thickness of the layers makes the numerical model computationally demanding due to the required high spatial and fine temporal discretization. To reduce the computation time, all the layers with thin thickness has been replaced with the "thin layer" assumption in the numerical model. The thin layer approximation approach provides promising results in modeling different physics related to superconductors by finite element analyses. Driesen et al. used thin layers for modelling thermal contact resistances and insulation layers in electrical machines [6]. De Sousa et al. used the thin-shell approach for modeling superconducting coated conductors [7]. The thermal thin shell approximation approach is also used for modeling thermal insulation layers in superconducting magnets in finite element quench simulation [8] and thermal insulation layers in accelerator magnets [9]. The basic principle behind the model for heater delay simulation is based on [10], and it is complemented here with associated NZPV simulation. The simulated heater delay and NZPV are validated with literature references [11], [12]. The model allows studying heaters with arbitrary lengths of heating stations. In future heater design it might be beneficial to use short heating stations which are optimal for high current operation and include only a few longer heater stations that are needed to protect the magnet at low current [12].

As a case study we used the CEA (French Alternative Energies and Atomic Energy Commission) R2D2 Nb₃Sn graded racetrack magnet [13], [14], see Fig. 1. A 2D longitudinal cross-section of
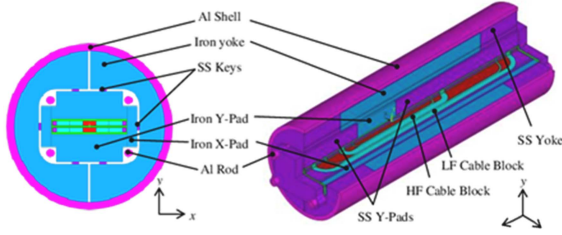
Fig. 1. Cross-section of R2D2 magnet and schematic of its mechanical components [13].
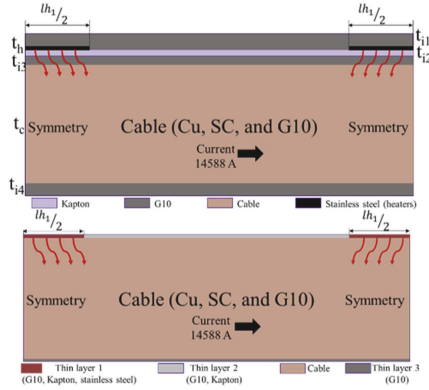

Fig. 2. Schematic of a 2D cable longitudinal cut with all material layers (up) and thin layer replacement (down).

TABLE I
THICKNESS OF LAYERS FOR 2D MODEL FROM TOP TO BOTTOM

Layer	Material	Thickness (mm)
Upper insulation layer (t_{i1})	G10	0.8
Heater (t_h)	Stainless steel	0.0254
Middle insulation layer 1 (t_{i2})	Kapton	0.05
Middle insulation layer 2 (t_{i3})	G10	0.15
Cable (t_c)	Nb$_3$Sn+Cu+G10	12.73
Bottom insulation layer (t_{i4})	G10	0.8

its high-field (HF) and low-field (LF) cables have been modeled using COMSOL Multiphysics software.

II. MATERIAL AND METHODS

A. Model Geometry and Materials

The schematic of a cable is illustrated in Fig. 2. The model consists of multiple material layers and heaters [15]. Between the heater and cable there is the heater insulation (Kapton) and cable insulation (G10) (respectively t_{i2} and t_{i3}). Heaters are covered with a G10 layer (t_{i1}), additionally, at the bottom there is a layer of G10 representing the cable and coil insulation. The thickness of each layer is summarized in Table I.

Thermal properties of the materials are temperature and magnetic field dependent. The cable is considered a homogenized mixture of copper, Nb$_3$Sn and G10. The average properties are determined with regards to the area fraction (A_i) for the thermal conductivity (K) and density (den) and mass fraction (m_i) for the specific heat (Cp). Equations (1), (2), and (3) represent

the equations used for the determination of density, thermal conductivity, and specific heat of the cable:

$$den_{cable} = \sum \frac{den_i * A_i}{A_{cable}} \tag{1}$$

$$K(T, B)_{cable} = \frac{K(T, B)_{Cu} * A_C}{A_{cable}} \tag{2}$$

$$C\,p(T)_{cable} = \sum \frac{Cp(T, B)_i * m_i}{m_{cable}} \tag{3}$$

where i corresponds to the materials in the cable (copper (Cu), Nb$_3$Sn, and G10). It is assumed that copper thermal conductivity dominates the cable thermal conductivity. The insulation layers are considered individually. An adiabatic boundary condition is assigned to the upper and lower boundaries. Tetrahedral mesh with 0.8 mm maximum size is applied to the entire geometry. The non-linear segregated iterative solver is used as the solver for the numerical simulation. The insulation layers and heater thickness within the thin layer have been discretized into 6 meshes.

B. Thermal Calculation

As represented in (4) thermal model includes the heat transfer by conduction in the system and the generated heat by the internal heat sources.

$$\rho C_p \frac{\partial T}{\partial t} - \nabla.(k\Delta T) = P \tag{4}$$

The heat sources are the heaters and the cable in its quenched regions. The heat generated by the heaters is determined by (5).

$$P_h\,(t) = \rho_{ss} * \left(\frac{I_{he} * e^{-\left(\frac{t}{\tau}\right)}}{t_h * w_h} \right)^2 \tag{5}$$

Where ρ_{ss} is the resistivity of stainless-steel heater at 4.2 K, t is time, τ is the current decay time constant, and w_h is the heater width. The exponential part of the (5) is related to the heater current decay. Joule heat in the cable (P_{JH}) is generated by the current flow in the copper after reaching T_{cs} (I_{Cu}) (6) [16]. We pre-calculate the current sharing temperature (T_{cs}) and critical temperature (T_c) based on the magnetic field, superconductor (SC) initial current density, and the critical current parameterization (J_c fit reference) [17]. Below T_{cs} no current is passing through the copper, and above T_c all the nominal current is passing through the copper [18]. Between T_{cs} and T_c, current is passing through the copper and Nb$_3$Sn which is so-called current sharing state of the cable.

$$P_{JH} = (1 + \cos(\alpha))^2 * (I_{Cu})^2 * \left(\frac{\rho_{Cu}(T)}{(A_{cable} * A_{cu})} \right) \tag{6}$$

I_{Cu} is the current passing through copper, ρ_{Cu}(T) is the copper resistivity, α is the cable pitch angle to account for the strand twisting [16], and A_{cu} is the area of the copper in the cable. I_{cu} and I_{sc} are determined by implementing a partial differential equation (PDE) in COMSOL. The copper resistivity depends on temperature, magnetic field and its RRR value. In this simulation the current distribution across the cable cross-section or among the strands is neglected, even if the magnetic field and

temperature would not be uniform in the cable cross-section in a real magnet.

C. Thin Layer Assumptions

Since the thickness of the insulation layers and heaters are significantly less than the thickness and length of the cable, they were modelled as a general "thin layer". In COMSOL Multiphysics, "thin layer" refers to a node that specifies the thermal conductivity and thermodynamic properties of a material present on internal or external boundaries [19]. The thin layer node may comprise a single material or a combination of multiple materials. Definition of the thin layer considerably reduces the calculation time by reducing the number of degrees of freedom (DOF) compared to the full model with all the layers. Thin layer approximation also reduces numerical instabilities while it can improve the accuracy of the results by giving freedom in mesh size selection. When the thin layer approach is used, finely surface meshed layer does not propagate its small mesh size to the rest of the model. This provides freedom in the selection of size while the mesh remains homogeneous and the same size. As represented in Fig. 2 three general type thin layers have been defined to replace the insulation and heater layers. In general type of the thin layer, both normal and tangential heat fluxes are considered. The thin layer could compromise several materials with different properties. Additionally, heat sources can be applied to specific sub-layers, as well as to the upper and lower sides of the layer.

- Thin layer 1: Consists of four layers: t_{i1}, t_{i2}, t_h, and t_{i3}.
- Thin layer 2: Consists of three layers: t_{i1}, t_{i2}, and t_{i3}.
- A single layer consists of layer t_{i4}.

As an example, for a 20 mm heater, a full model with all the layers has 234 780 DOF while the same model with a thin layer has 12 856 DOF. This means thin layer model has approximately has 18 times less DOF. This approach was verified by comparing the thin layer simulation with all material layers simulation, and the difference between the computed cable temperatures were within 0.1%. The computation time of the modeled case with thin layers is more than 10 times faster than the all-layer model.

D. R2D2 Magnet Operation Parameters

In this study for R2D2 we have considered the average magnetic field in LF and HF coil blocks at nominal current (6 T and 9 T), and heater total coverage and peak heater current (I_{he}) are considered constant. The influence of heater station length (l_h) on the temperature and resistivity of the cable has been investigated. Influence of magnet current (I_{nom}) and B on the NZPV have been investigated. A summary of the operating parameters and conductor characteristics is represented in Table II.

E. Normal Zone Propagation Velocity Model

To validate the NZPV calculation with experimental data from literature, and to investigate the NZPV behavior in the R2D2 cables, we did first simulations without powering the heaters. In order to remove the effect of generated heat by heaters on NZPV several modifications have been applied to the model

TABLE II
OPERATING PARAMETERS AND CONDUCTOR CHARACTERISTICS

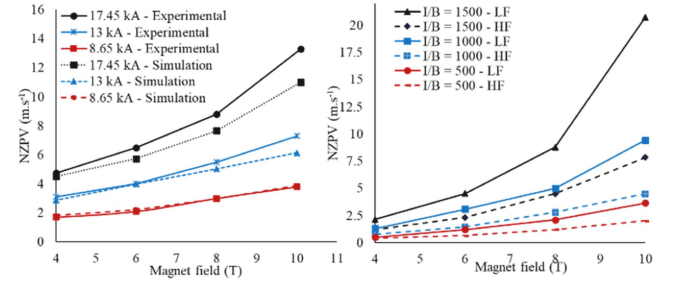|	HF	LF
I_{nom} at 4.2 K (A)	14588	
B (T)	9	6
RRR	200	450
c0 for J_c fit (A.(mm^2.T)$^{-1}$)	230984	195500
Strand diameter (mm)	1.1	0.7
Strand Cu/SC	0.9	1.8
Number of strands	21	34
$W_{cable} \times t_{cable}$ (mm^2)	12.73 × 2.06	12.73 × 1.31
T_c for I_{nom} = 14588 A (K)	12.6 at 9 T	13.76 at 6 T
T_{cs} for I_{nom} = 14588 A (K)	9.48 at 9 T	9.25 at 6 T
Cable pitch angle (°)	15	
I_{he} (A)	262	
$W_h \times t_h$ (mm^2)	30 × 2.54E-2	
Heater coverage	20 % of cable length	
τ (ms)	15	

Fig. 3. Comparison between NZPV determined by numerical simulation and experimental study in literature for MXQF coil [11] (left); NZPV for HF and LF cables for R2D2 magnet according to different current (right).

represented in Fig. 2: symmetry on the boundary on one side has been replaced with a fixed temperature slightly above the T_{cs} (T_{cs} + 0.5 K) – this is the start of the normal zone in the computation, furthermore, the thin layers 1 and 2 have been replaced by a single thin layer 3.

III. RESULTS AND DISCUSSION

A. Normal Zone Propagation Velocity Model Validation

In order to validate the numerical model for NZPV, we have used experimental results measured at CERN for the MQXF cable [11]. For this case the cable parameters were set to represent the MQXF cable. As represented in Fig. 3 (left), obtained results by numerical simulation have very good agreement with the experimental results especially at lower current and magnet field. The maximum value of error is about 18% at 17.45 kA and 10 T.

B. Normal Zone Propagation Velocity for R2D2

The NZPV for the R2D2 HF and LF cables is represented in Fig. 3 (right). The ratio of current to magnetic field is scaled linearly (1500, 1000, and 500) and four uniform magnetic field values from 4 T to 10 T have been simulated. At the same conditions LF cable has higher NZPV compared to the HF cable,
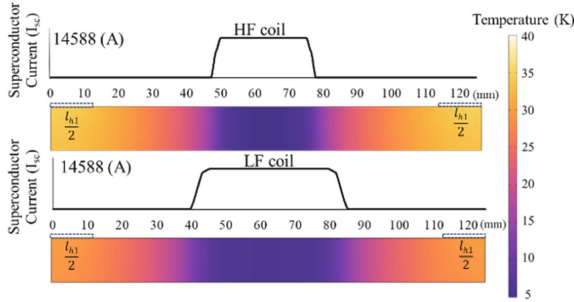
Fig. 4. Temperature in color and superconductor current for the LF and HF cable for a single heater (25 mm) at t = 22 ms.
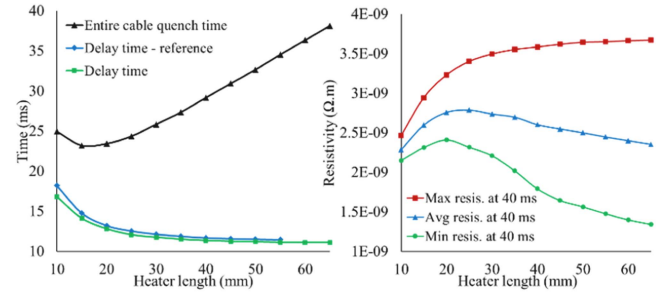

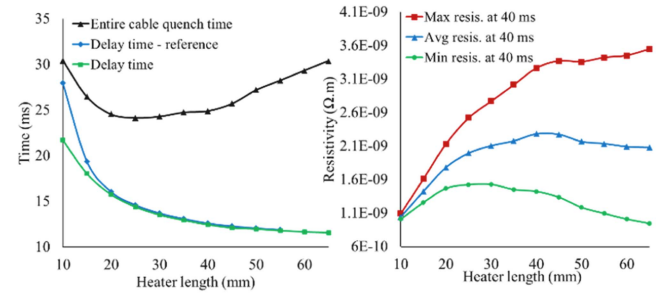Fig. 5. Influence of the heater length on the delay time (left), and cable resistivity (right) for the HF cable [12].

Fig. 6. Influence of the heater length on the delay time (left), and cable resistivity (right) for the LF cable [12].

because it has higher copper current density. For instance, NZPV of LF cable for 15 kA at 10 T is 20.74 m/s while it is 7.83 m/s for HF cable.

C. Protection Heater Performance Analysis

In this section, we consider a heater where all the heating stations have the same length. When the heater is fired, temperature of the cable gradually increases due to the energy provided by the heaters. Above the T_{cs}, the cable starts to generate Joule heat which soon becomes the main heat source and leads to a drastic increase of the temperature. Temperature distribution and SC current for a 25 mm long heater configuration at 22 ms after heater firing is represented in Fig. 4. In this case the distance between heating stations is 100 mm. At 22 ms the maximum temperature of the LF cable is 29.94 K which takes place at the closest point to the heater. This point is the first spot which undergoes quench in the cable. The minimum temperature of the LF cable is about 5.89 K which is at the farthest point in the cable from the heater center. On the HF cable, the maximum temperature is 34.82 K, and the minimum temperature is 5 K. One of the main reasons for the variation between cables is the difference in the copper area in the cables. The time to increase the cable temperature from T_{cs} to T_c is about 0.48 ms for LF cable and 0.31 ms for HF cable. In terms of space, the length of the current sharing regime is about 6.25 mm for LF cable and 2.73 mm for HF cable.

The influence of the heating station length on the heater delay (time to reach T_{cs} in the cable) was analyzed and compared with the literature reference [12]. The heater delay and the time to quench the entire cable is shown in Figs. 5 and 6. In our cases the distance between the heating stations is varied so that the heating station covers always 20% of the cable length. At the short heater lengths, discrepancies have been observed between the heater delay from the reference literature and the determined value in this article. This is mainly because in our case the distance between the heating stations is adjusted to keep 20% of the heating station coverage. In the reference case, the distance between heating stations is longer. The shorter period in our case is assumed to have led to a shorter delay for the shortest heating station lengths (10–20 mm).

In both cases, HF and LF cables, a heater length below 10 mm significantly increases the heater delay. On the other hand, for the

l_h above 35 mm for the HF cable and 45 mm for the LF cable, the influence of l_h on the quench delay is negligible. The same pattern is observed for maximum resistivity at 40 ms. Above these ranges, l_h does not highly influence the maximum temperature of the cable. The minimum time required for full quench of the cable (reaching T_c at the minimum temperature) for both cases is around 23–24 ms corresponding to 20 mm–30 mm heater for the HF cable and 35 mm–45 mm heater for the LF cable. The heater length beyond these ranges leads to an increase in the delay during which the cable is fully quenched between 2 stations due to the increase in the distance between the heating stations.

D. Consideration of Variable Heating Station Lengths

Created numerical model allows the optimization of the heater geometries that include different lengths of heating stations, such as the one envisioned in [12]. The full-scale optimization of real heater layouts is outside of the scope of this article, but we have shown here some examples of heater analysis. Obtained results represented in Figs. 5 and 6 show that for a single heater configuration with 25 mm heater station length leads to maximum average resistivity for HF magnet and 40 mm is the optimum for LF magnet – under the assumptions chosen for this article (neglecting real heater implementation and variation of the magnetic field among the cable turns). The optimum heater length for single heater configuration is compared to the two heaters configurations proposed in previous studies [12].

The variable heating station length configuration refers to the model with 6 heaters with different length (50 mm, 20 mm,
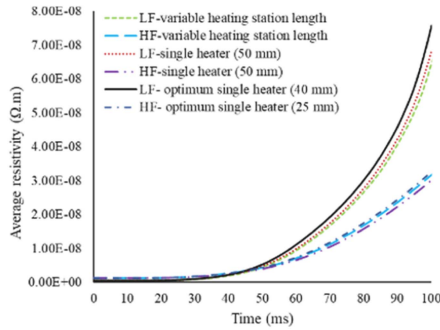
Fig. 7. Average resistivity for different heater configurations.

20 mm, 35 mm, 20 mm, 20mm). In this case, coverage percentage is 165 mm and total period is 825 mm and the distance between the heaters is 110 mm. Average cable resistivity with different heater configurations is shown in Fig. 7. Comparison between optimum configuration (25 mm for HF and 40 mm for LF) and 50 mm single heater indicate the marginal improvement of the resistivity in this heater station length range. In future, the resistivity calculation from this tool can be further used to compute the magnet current decay profile and the resulting peak temperatures. For example, it could be combined with an analytical method such as the one used in Coodi [20] and thus increase analysis accuracy.

IV. CONCLUSION

In this article, we introduce a COMSOL-based model developed to include the normal zone propagation modeling into the heater design workflow. To keep the computational time feasible, the model successfully employs the thin-layer approach, which was able to reduce the computation time by an order of magnitude compared to a COMSOL model with all insulation layers modelled individually. We have demonstrated the heating station placement impact on the cable resistance development for the coil average magnetic field. This model allows us to consider the aspect of quench propagation with more accuracy in the future for a full-scale heater optimization study. The next step is to use the full potential of this model and to perform full scale heater optimization studies for several magnets under design.

REFERENCES

[1] M. Benedikt and F. Zimmermann, "Towards future circular colliders," *J. Korean Phys. Soc.*, vol. 69, no. 6, pp. 893–902, Sep. 2016, doi: 10.3938/jkps.69.893.

[2] T. Salmi et al., "Quench protection challenges in long Nb₃Sn accelerator magnets," in *Proc. Adv. Cryogenic Eng.: Trans. Cryogenic Eng. Conf.*, 2012, pp. 656–663, doi: 10.1063/1.4706976.

[3] E. Ravaioli et al., "Quench protection studies for the high luminosity LHC Nb₃Sn quadrupole magnets," *IEEE Trans. Appl. Supercond.*, vol. 31, no. 5, Aug. 2021, Art. no. 4700405, doi: 10.1109/TASC.2021.3055160.

[4] T. Salmi et al., "Protection heater delay time optimization for high-field Nb₃Sn accelerator magnets," *IEEE Trans. Appl. Supercond.*, vol. 24, no. 3, Jun. 2014, Art. no. 4701305, doi: 10.1109/TASC.2013.2287634.

[5] G. Manfreda, G. Ambrosio, V. Marinozzi, T. Salmi, M. Sorbi, and G. Volpini, "Quench protection study of the Nb₃Sn low-β quadrupole for the LHC luminosity upgrade," *IEEE Trans. Appl. Supercond.*, vol. 24, no. 3, Jun. 2014, Art. no. 4700405, doi: 10.1109/TASC.2013.2285099.

[6] J. Driesen, R. J. M. Belmans, and K. Hameyer, "Finite-element modeling of thermal contact resistances and insulation layers in electrical machines," *IEEE Trans. Ind. Appl.*, vol. 37, no. 1, pp. 15–20, Jan./Feb. 2001, doi: 10.1109/28.903121.

[7] B. De Sousa Alves, V. Lahtinen, M. Laforest, and F. Sirois, "Thin-shell approach for modeling superconducting tapes in the H-φ finite-element formulation," *Supercond. Sci. Technol.*, vol. 35, no. 2, Feb. 2022, Art. no. 024001, doi: 10.1088/1361-6668/ac3f9e.

[8] E. Schnaubelt, M. Wozniak, and S. Schöps, "Thermal thin shell approximation towards finite element quench simulation," *Supercond. Sci. Technol.*, vol. 36, no. 4, Apr. 2023, Art. no. 044004, doi: 10.1088/1361-6668/acbeea.

[9] L. Bortot et al., "A 2-D finite-element model for electrothermal transients in accelerator magnets," *IEEE Trans. Magn.*, vol. 54, no. 3, Mar. 2018, Art. no. 7000404, doi: 10.1109/TMAG.2017.2748390.

[10] T. Salmi et al., "A novel computer code for modeling quench protection heaters in high-field Nb₃Sn accelerator magnets," *IEEE Trans. Appl. Supercond.*, vol. 24, no. 4, Aug. 2014, Art. no. 4701810, doi: 10.1109/TASC.2014.2311402.

[11] J. Fleiter, B. Bordini, A. Ballarino, L. Oberli, S. Izquierdo, and L. Bottura, "Quench propagation in Nb₃Sn Rutherford cables for the Hi-Lumi quadrupole magnets," *IEEE Trans. Appl. Supercond.*, vol. 25, no. 3, Jun. 2015, Art. no. 4802504, doi: 10.1109/TASC.2014.2367244.

[12] T. Salmi, D. Liu, V. Calvelli, and E. Rochepault, "Quench protection of Nb₃Sn high field magnets using heaters, a strategy applied to the graded racetrack dipole R2D2," *IEEE Trans. Appl. Supercond.*, vol. 33, no. 5, Aug. 2023, Art. no. 4701606, doi: 10.1109/TASC.2023.3251280.

[13] E. Rochepault et al., "3D conceptual design of R2D2, the research racetrack dipole demonstrator," *IEEE Trans. Appl. Supercond.*, vol. 32, no. 6, Sep. 2022, Art. no. 4004605, doi: 10.1109/TASC.2022.3158634.

[14] V. Calvelli et al., "R2D2, the CEA graded Nb₃Sn research racetrack dipole demonstrator magnet," *IEEE Trans. Appl. Supercond.*, vol. 31, no. 5, Aug. 2021, Art. no. 4002706, doi: 10.1109/TASC.2021.3075298.

[15] G. Manfreda, "Review of ROXIE's material properties database for quench simulation," CERN internal note 2011-24 1178007, 2011.

[16] A. Stenvall, T. Salmi, and E. Härö, "Introduction to stability and quench protection," in *Numerical Modeling of Superconducting Applications*, vol. 4. Singapore: World Sci., 2023, pp. 107–185.

[17] EuroCirCol, "16T dipole design options: Input parameters and evaluation criteria," EuroCirCol-P2-WP5, Sep. 2015. [Online]. Available: https://indico.cern.ch/event/441684/

[18] L. Bottura and O. Zienkiewicz, "Quench analysis of large superconducting magnets. Part I: Model description," *Cryogenics*, vol. 32, no. 7, pp. 659–667, 1992, doi: 10.1016/0011-2275(92)90299-P.

[19] COMSOL Multiphysics, "Theory for heat transfer in thin structures," Heat Transf. Module User's Guide, 2018. [Online]. Available: https://doc.comsol.com/6.1/docserver/#!/com.comsol.help.heat/heat_ug_theory.07.031.html%23643224

[20] T. Salmi et al., "Quench protection analysis integrated in the design of dipoles for the future circular collider," *Phys. Rev. Accel. Beams*, vol. 20, no. 3, Mar. 2017, Art. no. 032401, doi: 10.1103/PhysRevAccel-Beams.20.032401.